Building a geochemically-constrained time-varying eruption hazard forecasting model for Mt Taranaki

Final Report

12 May 2009

Shane J. Cronin, Michael B. Turner, Mark S. Bebbington,
Volcanic Risk Solutions, Massey University, Private Bag 11 222, Palmerston North

Summary:

In this report we present our latest work on the development of a time-varying eruption hazard forecasting model for Mt. Taranaki. The goals of this work are twofold: to develop a probabilistic forecast model that takes into account the underlying magmatic system; and to achieve integration between geochemical-based interpretations and statistical approaches based on high-precision temporal records of eruption events.

The success of this project relied on the development of a most-complete volcanic history record of Mt. Taranaki. This was achieved by using pumice-bearing tephra layers (indicative of fast- ascending magmas which led to the production of high eruption columns of sub-plinian eruptions). Sites along only one dispersal direction were sampled, assuming a long-term even probability of ashfall in this direction. From this record, an annual eruption rate was calculated. This rate revealed that a regular periodicity in eruption frequency has occurred over the Holocene. A hypothesis proposed before this study was that magma recharge events were behind eruption frequency cycles at Mt Taranaki. These recharges are events that move fresh magma from the base of the crust (25 km) to mid crustal (7-10 km) reservoirs. Identified recharge events (evidenced within crystals of plagioclase and titanomagnetite within tephras), however, show no relationship to eruption cycles. Hence this hypothesis was rejected.

This study discovered that another magmatic feature appears to control eruption frequency. Geochemical evidence with titanomagnetite and glass chemistry, as well as whole-rock trace-element chemistry, showed that over the Holocene period, eight distinctive “batches” of magma were erupted. Each of these batches produced magmas of progressively evolving compositions over a period of c. 1500 years. The timing of magmatic batches clearly matches eruption frequency, with highest eruption rates near the mid-point of each batch “life”. With the aid of petrological, geochemical and geophysical data, a model consisting of a lower crustal zone is used to explain the geochemical and subsequent eruption cycles. Each cycle is the result of mantle-sourced intrusions into a lower crustal sill/dyke complex. The intruded melt undergoes 1500 years of assimilation, fractionation and crystallisation processes and residual melt from these cooling bodies periodically rises to feed the upper magma storage region (producing the recharge signature of the phenocryst assemblage). Superimposed on this 1500-yr cyclic trend is that fact that from ~3000 yrs BP Taranaki’s magma composition has included a much greater mafic component, associated with development of the satellite cone of Fanthams Peak.

In addition, the largest known Holocene eruptions from Mt Taranaki occur regularly in the trough of the eruption frequency curve, coinciding with the end of a compositional magma batch. These largest events are uniformly the most evolved (silicic) andesites. These datasets illustrate the relationship between the magma system and eruption frequency, and are therefore important for constraining the timescales and nature of the magmatic processes. Using Hidden Markov statistical models we can now quantify the eruption variability and therefore provide a more realistic probabilistic eruption forecast.

1. Treatment of radiocarbon ages

Some of the results and models presented here are a reflection of those given in our last report in June 2008. However, there is one fundamental difference: the use of radiocarbon years verses calibrated calendar years.

Raw radiocarbon years are not equal to true calendar years because they relate to the amount of Carbon-14 within the Earth's atmosphere which has not been constant throughout time. Therefore raw radiocarbon years cannot be used directly as a calendar age. Radiocarbon dates, in B.P. years, are calibrated to give calendar ages. Standard calibration curves are available for each hemisphere, based on comparison of radiocarbon dates of samples that can be dated independently by other methods such as tree rings (dendrochronology) or deep ocean sediment cores (McCormic et al. 2004, Reimer et al. 2004, Stuiver and Pearson 1992). The differences between the radiocarbon years and calendar years are illustrated in Figure 1.

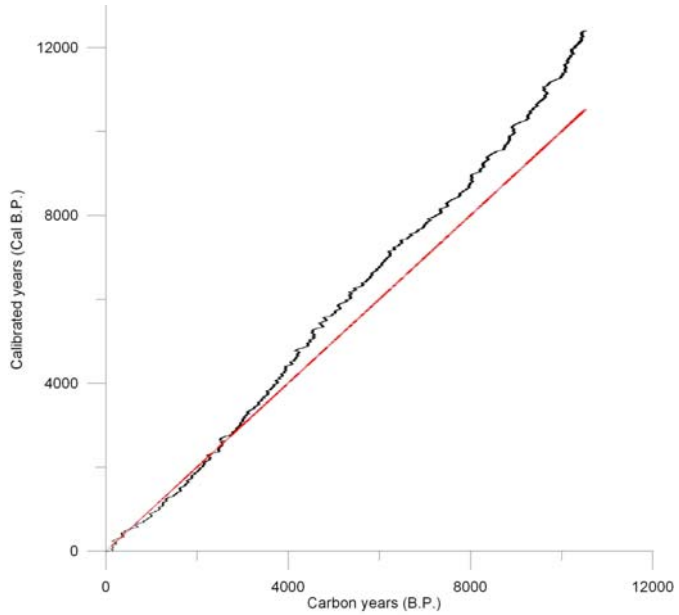

Figure 1 The southern hemisphere calibrated radiocarbon curve (McCormic et al. 2004) in black, plotted with the 1:1 ratio between Carbon years and Calendar years (in red).

Normally distributed errors are associated with radiocarbon years and are the result of counting statistics of Carbon-14 during analysis (Stuiver and Pearson, 1992). In contrast, the conversion of a radiocarbon age to that of a calendar year will produce a date that has significantly larger errors associated with it. These errors are due to the variation of the atmospheric carbon fraction with time, resulting in irregular fluctuations of the radiocarbon to calendar year curve (Fig. 1). In addition, the calibrated curve also contains a normal standard error associated with the radiocarbon dating of the known calendar year material (Fig 2). A single radiocarbon date with normally distributed errors may overlap the calibrated curve at a number of points, resulting in a date with much more complicated errors. This is clearly illustrated in Figure 2

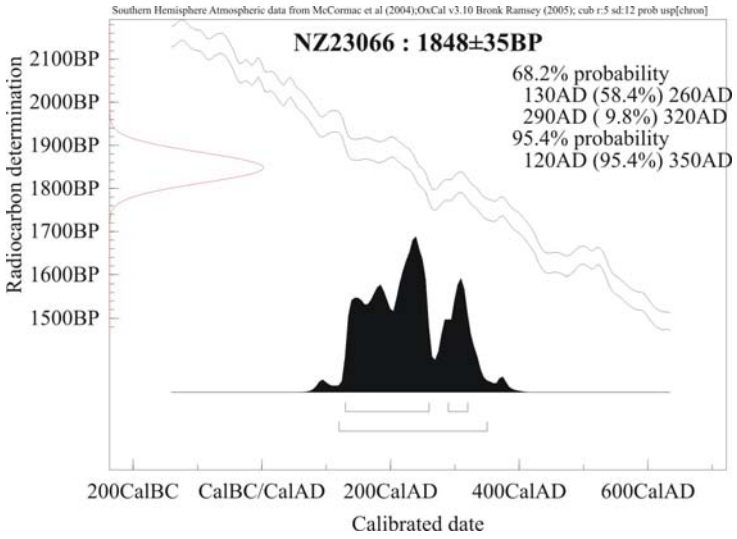

Figure 2 Calibration of radiocarbon date NZ23066 (years B.P.) to Calendar years (A.D.) years using OxCal v.3.10 (Brook-Ramsey 2003)

In Turner et al. (2008a) a depth to age profile of the cores were used to assign radiocarbon ages to all of the individual tephras. This database was subsequently used in eruption recurrence analysis and forecast models. The radiocarbon ages were initially used because they have relatively simple errors associated with them. Re-sampling can be made from within these error distributions; polynormals fitted, and interpolated dates obtained (Fritsch and Carlson 1980). Repeating the re-sampling procedure many times while maintaining the stratigraphic order will give interpolated dates with similar errors to those associated with radiocarbon dates (Turner et al. 2008a). However, since radiocarbon ages are not true years before present, eruption predictions cannot be accurately made. We assumed that the forecasted probability using the radiocarbon event database could be overstated by up to 14% because of the slightly longer timeframe (i.e., 6250 years B.P. calibrates to 7220-7050 Cal. years B.P; Fig. 2).

In Turner et al. (2008b) the radiocarbon event database was smoothed into a probability of events per year function. A 1500-2000 periodicity of eruption frequency was revealed by this data analysis. The observed variations in eruption frequency were assumed to be real because they were observed over a relatively large time frame (c. 11 000 years B.P.), and so the difference between carbon years B.P. and calendar years B.P. was not so significant (i.e., Fig. 1).

We have since been able to run the re-sampling procedure and subsequent analysis using calibrated calendar dates by starting the analysis at the youngest date and subsequently re-sampling between dates and events, making sure that each event still preserves the correct stratigraphic order. The resulting probability curve of events per year clearly illustrates that our assumption was valid and the volcano has a strong cyclic eruption periodicity.

2. Integrating geochemical and probabilistic models

This aspect of our research is encapsulated in a full manuscript that is in its last drafting stages before submission to the journal “Earth and Planetary Science Letters”. The manuscript is included in full in this report as Appendix 1.

3. Probabilistic Eruption Forecast Models:

The first eruption forecasts for Mt Taranaki were published in early 2008 in the Bulletin of Volcanology paper: Turner MB, Cronin SJ, Bebbington MS, Platz T (2008a) *Developing probabilistic forecasts for dormant volcanoes: a case study from Mt. Taranaki* Bull Volcanol 70: 507-515. This paper attempted to produce a probabilistic eruption forecast using best-fit renewal models from a detailed record of tephra fall within Lake Umutekai. The result of this study provided a probability of at least 0.37-0.48 for a new eruption from Mt Taranaki in the next 50 years.

Tephra dispersal is, however, highly variable depending on the dominant wind strengths and direction(s) and therefore not all tephra-producing eruptions may leave a deposit at a single location. It is therefore assumed that this first probabilistic forecast provides only a minimum probability. Turner et al. (*in press*) produced a combined dataset from two different lake sites (Lakes Umutekai and Rotokare), and an edifice record of 23 events whose deposits are dated between 96 - 2200 years B.P. In total there are 169 events from all three records. A method consisting of two techniques for correlating syn-eruptive deposits was developed. Firstly, tentative matches were identified using the radiocarbon age and associated error of each event. Secondly, the compositions of titanomagnetite micro-phenocrysts were used as an independent check. The final combined dataset suggests that there have been at least 138 separate tephra-producing eruptions between 96 and 10 150 years B.P. from Mt Taranaki. As with the earlier study (Turner et al. 2008a) a mixture-of-Weibulls renewal model was used to estimate an accurate probabilistic eruption forecast for Mt. Taranaki. Using the combined eruption record and the mixture-of-Weibulls model, an estimate of 0.52 is made for the probability of an eruption occurring within the next 50 years. This estimate is 1.5 times that of the previous one derived from the single site record (i.e., 0.37; Turner et al. 2008a).

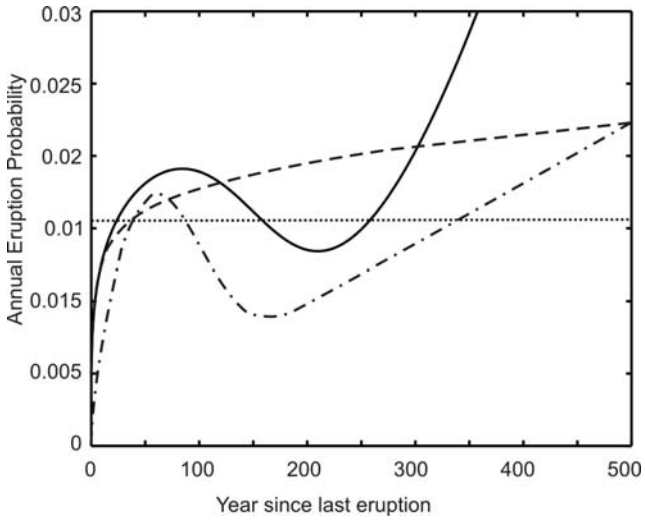

Figure 3: Annual eruption probabilities. Dotted line = exponential distribution, dashed = Weibull, solid = mixture-of-Weibulls, dot-dashed = mixture-of-Weibulls (Turner et al. 2008a).

The distribution of events over time from the combined record reveals a peak interval renewal interval of approximately 16 years and a second more diffuse renewal period of 232 years (the cause of the 'dip' in Fig 3). This bi-modal distribution of events provides further evidence that there is some cyclic structure to the eruption frequency from Mt. Taranaki. Indeed, these longer repose periods may represent those periods where the volcano is erupting less frequently, consistent with the 1500 year periodicity in the frequency of explosive eruptions on which much of this current EQC research has focused.

To provide relatively better constrained, and therefore more realistic, probabilistic eruption forecasts, the forecast model needs to account for the eruption frequency variability. Hidden Markov models provide the means to quantify these observations (Bebbington 2007).

3.1 Hidden Markov model

Hidden Markov models allow the distribution of time between events (reposes) to depend on an unobserved, or hidden 'state variable'. The repose lengths will have Weibull distributions with different parameters for each identified repose state. The state variable evolves from repose to repose as a Markov chain. The number of hidden states is selected using the Akaike Information Criterion (AIC = -2 log L + 2k), which balances the degree of fit against the number of parameters to avoid over fitting. For the combined dataset of Turner et al. (*in press*) the mean dates of events within the 6250 years B.P. – present dataset were used (i.e., the part of the record where there is more than one site). The process of accounting for hidden state intervals in probabilistic eruption forecasts is given in Figures 4 to 8.

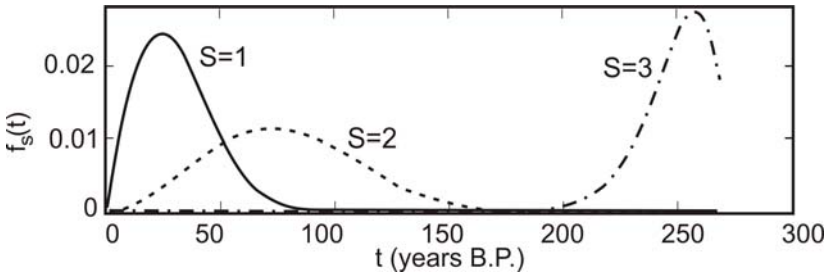

Figure 4: Repose length distributions, indexed by state S. There are short, medium and long repose regimes observed (i.e., mean repose period of state 1 is approximately 25 years, whereas the mean repose period of state 3 is approximately 260 years).

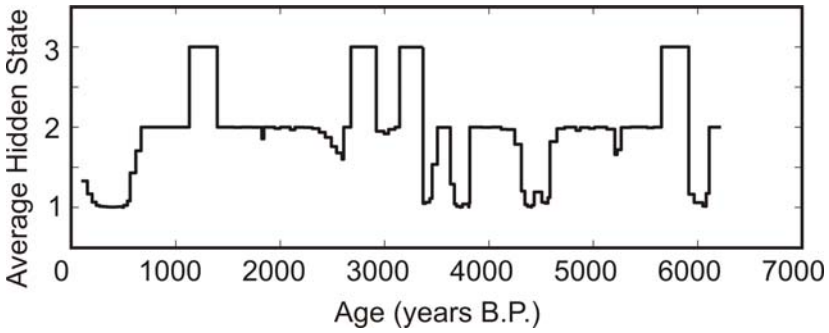

Figure 5: Estimated hidden state path (3 = long, 1 = short repose) from the combined record of Turner et al. (*in press*).

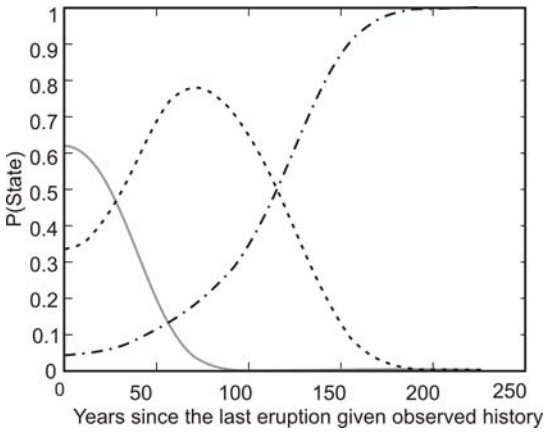

Figure 6: Probability of being in a given state (i.e., that the present repose is from that class). This is found when the time since the last event is accounted for, using the observed history (Fig 5) of the volcano. S = 1 (Solid grey line), S = 2 (Dashed line), and S = 3 (dot-dash line).

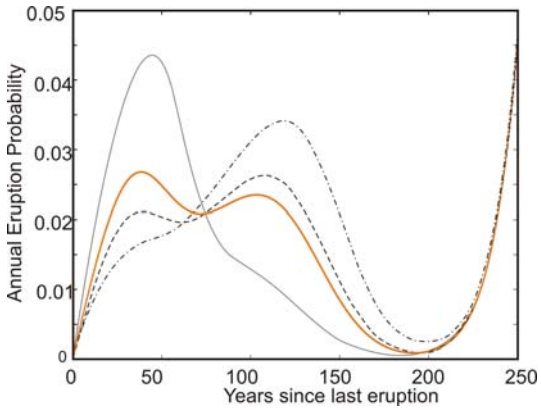

Figure 7: Annual eruption Probability. The grey solid, dashed and dotted lines are when the state at the last eruption was 1, 2 and 3 respectively, which is unknown. The probabilities given in Fig 6 allows the weighted average to be calculated (orange line).

Applying Hidden Markov models to the combined dataset confirms that there is strong structure to the eruption frequency of Mt. Taranaki with times where either short or long repose periods dominate (Fig. 5). These periods appear to alternate on a 1000 – 2000 year timescale that is in agreement with the observations of Turner et al. (2008b) and the outcomes of this EQC funded research. The result of this research incorporates the identified time-varying eruption periodicity of Mt Taranaki into a probabilitistic hazard forecast estimate and therefore provides our best-yet estimate of future activity from Mt Taranaki (Fig 8).

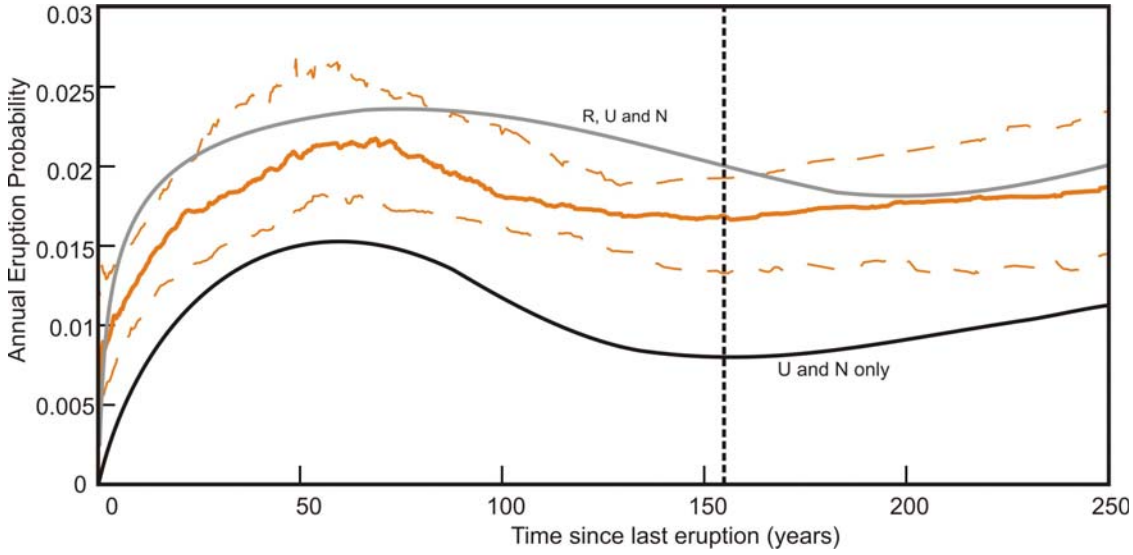

Figure 8: Incorporating the estimated error in the eruption dates into the procedure using a three state Hidden Markov model. The solid orange line is the median of 200 Monte Carlo runs; the orange dashed lines are the lower and upper quartiles. For comparison, the annual eruption probability acquired by the best fitted renewal models is also given. Umutekai (U) and near-source (N) datasets only (black-line; from Turner et al. 2008a) and the combined records that includes the Rotokare (R) datasets (grey line: from Turner et al. *in press*). Vertical line indicates the present day hazard.

4. Avenues for future research

The outcomes of this study provide important observations of timescales associated with the magmatic processes operating at Mt Taranaki. However, it is recognized that this work is only a step along the way to understanding the overall magmatic processes of andesitic volcanism, and hence providing accurate assessments of this future risk. There are many aspects that would benefit from further, focused study. The following avenues of research would contribute to a more comprehensive knowledge of the volcanic processes at volcanoes such as Mt Taranaki and strongly improve the quality of time-varying eruption prediction models.

1) Although the eruption record of Turner et al. (*in press*) is the most complete record to date, the record only reliably goes back to 10 000 yrs B.P. Gaining accurate records of tephra producing eruptions prior to the Holocene period will provide an opportunity to observe possible longer-term trends in magma processes and eruption frequency. In addition, how does basaltic volcanism, specifically eruptions from Fanthams Peak, fit into the eruption frequency of the volcano? Evidence from Turner et al. (*in press*) suggests that the initiation of Fanthams Peak occurred at approximately 3000 years B.P. However, on-

edifice soil profiles contain basaltic material at horizons >10 000 years B.P. Does this imply that there have been similar parasitic vents?

In 2005, a professional drilling-rig was employed to obtain an 18 m length, 10 cm diameter core from the Eltham Swamp (Fig. 9). The sediment substrate of the core is mostly fibrous peat and hence there is a coarser lower limit on the thickness of tephra that can be preserved within it compared to lake sediments (i.e., > 5 mm compared to c. 0.5 mm). Michael Turner's PhD project therefore concentrated on the more detailed cores obtained from Lakes Rotokare and Umutekai. Since the completion of this initial research we have been focusing our attention on the Eltham Swamp core. In November 2008 we sub-sampled the core for radiocarbon dating and were surprised to discover that the core extends the record of 168 explosive eruptions back to the formation of the swamp by a volcanic debris flow at 32 000 years B.P. From the 7 dates we obtained throughout the length of this core, an initial eruption frequency analysis suggests that at approximately 24 000 years B.P. there was a period of approximately 500 years where an abnormally high rate of eruptions occurred. Further dates are needed so that an accurate age/depth curve can be constructed that will allow for a better constrained frequency analysis. In addition, each tephra has been sampled from this core and processed in readiness for geochemical analysis.

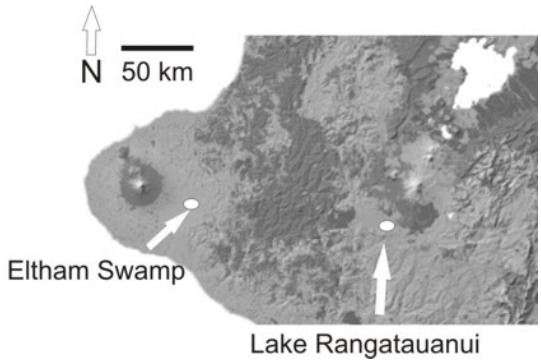

Figure 9: Map of the central North Island showing the locations of sample sites Eltham Swamp and Lake Rangatauanui

2) Acquiring eruption records from more distal sites (such as lake and swamp sites) will provide valuable data for modeling the attenuation and dispersal characteristics of widespread tephra producing eruptions. These models are needed so that an estimate of ash-fall thickness can be obtained for any given site down-wind from the volcano.

   As part of Ms Anja Moebis' PhD research (who is also funded by an EQC fellowship) we obtained a core from a small lake near the township of Ohakune; Lake Rangatauanui (Fig. 9). Within the 3.5 metre core, extending back 18 000 yrs B.P., there were over 100 individual tephras identified. Ms Moebis has sub-sampled this core and obtained geochemical data from each tephra. Many tephras derived from Mt Taranaki have been discovered. Lake Rangatauanui lies along the same dispersal axis to the Eltham Swamp. Once geochemical data can be obtained for the tephras of the Eltham Swamp core they may then be correlated to those found in the Rangatauanui core, using the techniques identified in Turner et al. (*in press*). This work would then allow us to quantify the attenuation of volcanic ash from Mt Taranaki.

3) Although the use of Hidden Markov models have been able to quantify the 1500 year periodic structure within the eruption frequency for a more accurate probabilistic hazard estimate, the database we used in the Hidden Markov model process incorporates all events from three sites. An important issue is that although this is the most complete eruption record yet, it is still incomplete due to the restricted distribution of ash fall from dome collapses (Block-and-ash flow events; BAF). It is therefore likely that we are missing the true number of these events from our record. To overcome this obstacle we could constrain the average frequency of these events in the most accurately identified and dated period

known from Mt Taranaki over the last 800 years B.P. (Platz 2007). This window of activity could then be 'scaled up' to constrain estimates of the 'missing' parts of the volcanic records. Unfortunately, if we use this method we will be unable to identify any variability in the frequency of such events. Because BAF producing eruptions have unique hazards associated with them, this lack of knowledge hinders the development of comprehensive probabilistic forecasts. To overcome this obstacle, we need to understand the processes and the timescales of processes that drive all different eruption styles at andesitic volcanoes.

5. References cited:

Bebbington MS (2007) Identifying volcanic regimes using hidden Markov models. Geophys J Int 171:921-942

Bronk-Ramsay C (2003) Oxcal Program v. 3.10: Oxford Radiocarbon Accelerator Unit, Oxford, UK.

Fritsch FN, Carlson RE (1980) Monotone piecewise cubic interpolation. SIAM J Num Anal 17: 238-246.

McCormack FG, Hogg AG, Blackwell PG, Buck CE, Higham TFG, Reimer PG (2004) SHCal04 Southern Hemisphere calibration, 0-11.0 cal kyr BP. Radiocarbon 46: 1087-1092.

Platz T (2007) Aspects of Dome-forming Eruptions from Andesitic Volcanoes through the Maero Eruptive Period (1000 yrs B.P. to Present) Activity at Mt. Taranaki, New Zealand. Unpub PhD thesis, Institute of Natural Resources, Massey University, Palmerston North, New Zealand.

Reimer PJ, Baillie MGL, Bard E, Bayliss A, Beck JW, Bertrand CJH, Blackwell PG, Buck CE, Burr GS, Cutler KB, Damon PE, Edwards RL, Fairbanks RG, Friedrich M, Guilderson TP, Hogg AG, Hughen KA, Kromer B, McCormac G, Manning S, Bronk-Ramsey C, Reimer RW, Remmele S, Southon JR, Stuiver M, Talamo S, Taylor FW, Van der Plicht J, Weyhenmeyer CE (2004) INTCAL04 Terrestrial radiocarbon age calibration, 0-26 Cal kyr BP. Radiocarbon 46: 1029-1058.

Stuiver M, Pearson GW (1992) Calibration of the 14C time scale 2500-5000 BC. In: Taylor RE, Long A, Kra RJ (eds) Radiocarbon dating after 4 decades: an interdisciplinary perspective, Springer, New York, pp. 19-33.

Turner MB, Bebbington MS, Cronin SJ, Stewart RB, (in press) Merging Eruption Datasets: Towards an Integrated Holocene Eruptive Record of Mt Taranaki, New Zealand, Bull Volcanol. accepted December 2008.

Turner MB, Cronin SJ, Bebbington MS, Platz T (2008a) Developing a probabilistic eruption forecast for dormant volcanoes; a case study from Mt. Taranaki, New Zealand. Bull Volcanol 70: 507-515. DOI: 10.1007/s00445-007-0151-4.

Turner MB, Cronin SJ, Smith IEM, Bebbington M, Stewart RB (2008b) Using titanomagnetite textures to elucidate volcanic eruption histories. Geology 36: 31-34.

Turner MB (2009) Eruption cycles and magmatic processes at a reawakening volcano, Mt. Taranaki, New Zealand. Unpub thesis, Institute of Natural Resources, Massey University, Palmerston North, New Zealand

Appendix 1:

Manuscript in preparation for submission to "Earth and Planetary Science Letters"

Understanding Magma Batch Production at Andesitic Volcanoes: a case study from Mt. Taranaki, New Zealand

Michael B. Turner[1], Shane J. Cronin[1], Mark Bebbington[1],

[1.] *Volcanic Risk Solutions, Institute of Natural Resources, Institute of Fundamental Sciences, Massey University, Private Bag 11 222, Palmerston North 4442 , New Zealand*

Abstract:

The eruption records of andesitic strato-volcanoes are inherently complex, but they often indicate decadal periods of intense activity, followed by centuries of only intermittent events. Acquiring accurate eruption records and understanding the volcanic processes behind eruption intervals are important to the development of realistic hazard assessments and volcanic emergency planning. A detailed study of Mt Taranaki's Holocene eruption record provides clarity to magmatic processes of andesite volcanoes and helps to demystify these seemingly complex volcanoes.

Compositional profiles and zoning textures of plagioclase, amphibole and clinopyroxene phenocrysts of Mt Taranaki eruptions give evidence of magma reheating and/or recharge of the upper magma storage region. These recharge events appear to occur on varying decadal to century timescales. In contrast, the relatively fast elemental diffusion rates within titanomagnetites mean that the proportions of Al, Mn and Mg, for example, reflect variations in surrounding melt composition (and to a lesser degree the magma temperature and fO_2) on shorter time scales. For most of Mt Taranaki's Holocene history, titanomagnetite compositions and element data display distinctive 1500-2000 year cycles. Most importantly, these cycles correspond extremely closely with the overall eruption event frequency curve for Taranaki. We suggest that a developing lower crustal hot zone is the cause of these cycles, with each cycle being the result of mantle-sourced intrusions into a lower crustal sill/dyke complex. The intruded melt undergoes 1500 years of assimilation, fractionation and crystallisation (AFC) processes and residual melt from these cooling bodies periodically rises to feed the upper magma storage region. Confirming a relationship of magma compositional cycles to the eruption frequency at volcanoes such as Mt. Taranaki is important for constraining the timescales and nature of magmatic processes, as well as being a key foundation for time-varying hazard assessments for andesitic volcanoes.

1. Introduction

Following the 1980 eruption of Mt. St Helens petrology and physical volcanology studies were integrated in the first meaningful way to understand eruption processes and magma rise and eruption (Lipman and Mullineaux 1981; Cashman and Taggart 1983; Carey and Sigurdsson 1985).

With the development of high-precision, micro-geochemical techniques and isotope analyses (Turner et al. 2001; Zellmer et al. 2003; Condomine et al. 2003), together with detailed modelling (Zellmer et al. 1999; Costa et al. 2003; Morgan et al. 2004), geochemical studies are now able to provide precise constraints for the location and timescales of magma differentiation. However, difficulties remain in the integration of these findings into holistic and long-term models of eruption recurrence at re-awakening volcanoes. One of these is the acquisition of comprehensive eruption records that are long enough to smooth out any short-term anomalies in eruption history. Another is developing an equally comprehensive and time-constrained view into the magmatic system of the volcano.

Historic eruption activity from some of the world's best documented intermediate and siliceous volcanoes show semi-regular periods of volcanic activity separated by intervals of quiescence (e.g., Vesuvius: Scandone et al. 1993; Merapi: Andreastuti et al. 2000; Fuji: Miyaji 1988). In this paper we use geochemical data from an extremely precise Holocene eruption record of the andesitic Mt. Taranaki (New Zealand) to demonstrate a genetic link between regular cycles of magmatic evolution and variations in the eruptive frequency of the volcano. The resulting detailed geochemical observations from this record are used to discuss the possible causes of the periodic magmatic evolution.

2. The Holocene eruption rate of Mt. Taranaki

2.1 Mt. Taranaki

Mt. Taranaki, western North Island, New Zealand (Fig. 1), is typical of arc-related systems throughout the world, with Holocene eruptions comprising mostly basaltic-andesite to dacite magmas (Stewart et al. 1996). Summit-sourced eruptions are generally andesitic to dacitic, while those from the parasitic Fanthams Peak are typically basaltic andesite. Although Mt. Taranaki has been in a state of quiescence for at least 150 years, edifice and ring-plain deposits indicate a complex history of frequent explosive volcanism, dome construction and lava-extrusion (Neall et al. 1986), similar to a number of recently active volcanoes, such as: Unzen (Japan), Merapi (Indonesia), and Augustine (Alaska). Like many dormant volcanoes, prehistoric eruption records and geochemical studies have largely concentrated on easily identifiable and accessible deposits (Neall et al. 1986; Alloway et al. 1995). Although these provide the basic framework for geochemical models of magma genesis (Price et al. 1999) and eruption frequency for larger eruptions (Alloway et al. 1995), this preliminary work does not contribute to our understanding of the shorter term (months to centuries) eruption record or the magmatic processes responsible for this more-typical activity. To rectify this, a high-precision temporal eruption record for Mt Taranaki was constructed from lacustrine and peat swamps surrounding the volcano (Turner et al. in press) and used to define the sampling regime for the geochemical aspects of this study. Lake Umutekai, lying 25 km NNE from the summit of Mt. Taranaki (Fig. 1) provided a key location for this study. In a four metre core from this lake, 103 individual tephra layers were recognised between c. 1500 to 10 500 yrs B.P. Each tephra layer from these cores was assigned a unique age (with associated normally distributed errors) from a spline-fit, core-depth function calculation, interpolated from 9 radiocarbon dates for Umutekai (Turner et al. in press).

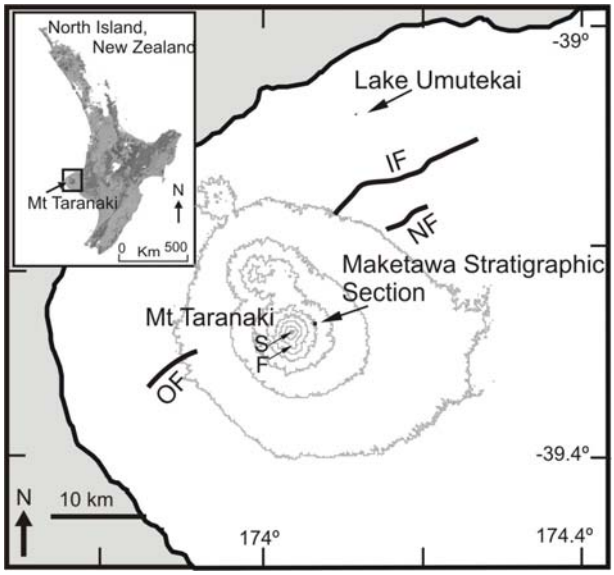

Figure 1: *Map of the Taranaki region showing the locations of the sample sites, Lake Umutekai and Maketawa Stratigraphic Section. 300 m contours shown in grey with the >1500 m highlighted. (S) Summit vent, (F) Fanthams Peak vent. There are three active oblique normal slip NE-SW-trending faults of the Taranaki region: the Oaonui Fault (OF), Inglewood Fault (IF), and Norfolk Fault (NF). Insert: North Island, New Zealand.*

2.2 Eruption frequency analysis

For eruption frequency analyses, combining multiple records from various locations that cover various time ranges (Turner et al. in press) may involve variable levels of bias. A single-site record may be more suitable, because if wind patterns have a constant degree of variability, the sampling probability of the single site will remain the same. Hence, eruption frequency analysis was performed on the Lake Umutekai record. This lake lies near the major NE tephra fall dispersion axis and during the Holocene insignificant changes to the overall high level winds occurred (c.f., Alloway et al.1995). This means that there was a near-constant probability that during a widespread eruption, ash would have been deposited at this site. To reduce a second form of bias created by the restricted distribution of ash fall from dome collapses, only eruptions producing high central columns were considered. Such eruptions are most likely to be from fast-ascending magma, producing sub-plinian style eruptions and thus are represented in the geological record as pumice-rich fall layers. Pumice-bearing deposits within this record were identified by a combination of glass and titanomagnetite observations (Turner et al. 2008a).

The upper part of the lake record was unobtainable due to the uppermost sediment column being unconsolidated. To complete the eruption record, Turner et al. 2008b used a database of well dated events from near-source deposits. However, most of this 'recent' record relied on the dating of block-and-ash flow deposits produced during dome building eruptions. To overcome these problems and therefore complete the record of sub-plinian eruptions, an edifice site was used (Maketawa Stream; Fig. 1). At this site block-and-ash-flow and fall deposits are preserved, with intervening paleosols and medial ash. The Maketawa Stream site is ideally situated, directly between the summit and Lake Umutekai (Fig. 1) and it contains two marker horizons: a well recognised pumice-bearing pyroclastic deposit of the AD 1655 Burrell eruption (Druce 1966) and a charcoal bearing block-and-ash-flow (NZ-16391; 1130 ± 34 yrs B.P.).

Table 1: *Largest known explosive pyroclastic eruptions (>0.6 km^3) from Mt. Taranaki. The named tephras and associated dates are described by Neall (1972). Largest tephras identified within the Lake Umutekai record (>1 cm and mean grain size >250 µm). In addition, Mt. Taranaki tephras identified within lakes of the Waikato district (Lowe 1988) are listed.*

Tephra name	Age (yrs B.P.)	Data code	Source	Lake Umutekai tephra no.	Interpolated age (yrs B.P.)	Tephra (Lowe 1988)	Age (yrs B.P.)[d]
Burrell Lapilli	300 ± 60	NZ63	Fergusson and Rafter (1957)				
Kaupokonui Tephra	1390 ± 150	NZ6508A	Lees and Neall (1993)				
				8[b]	2237 ± 24		
				9[b]	2368 ± 30	Eg-1[c]	2500
Maketawa Tephra	2890 ± 100	NZ3423A	Alloway et al. (1995)				
Manganui Tephra	c.3100[b]		Alloway et al. (1995)				
Inglewood Tephra (a)[a]	3610 ± 80	NZ3353A	Neall (1979)			Eg-2	3700
Inglewood Tephra (b)[a]	3690 ± 80	Wk-1031A	Alloway et al. (1995)	25	3722 ± 39	Eg-3	3750
Korito Tephra	>4150 ± 100	Wk-1033A	Alloway et al. (1995)	33	4311 ± 36	Eg-4	4100
Tariki.e	4590 ± 100	Wk-1034A	Alloway et al. (1995)	34	4346 ± 38	Eg-5	4400
Wakipuku Tephra	5260 ± 90	Wk-1035A	Alloway et al. (1995)			Eg-6	5250
						Eg-7	5850
						Eg-8	5900
Kaponga.f	8947 ± 130	NZ7986A	Hull (1994)				
						Eg-9	9300
						Eg-10	9600
Konini.b	10 150 ± 100	NZ3153A	McGlone and Neall (1994)			Eg-11	10100

[a]Divided into two tephras on the bases of radiocarbon ages and the description of a 'medial interbed <0.14m thick' separating the two (see Alloway et al. 1995).
[b]Fanthams Peak eruptive. Estimated age based on sediment thickness between radiocarbon dates (NZ3423A) of 2890 ± 60 and (NZ3139A) of 3320 ± 60 yrs BP (McGlone et al. 1988).
[c]Likely to be part of the 'Manganui tephra' based on the radiocarbon age compared to Manganui tephra found in the Umutekai record.
[d]Most dates interpolated between two radiocarbon dates acquired directly above and below the sampled tephra. Some are interpolated from the sedimentation rate (see Lowe 1988).

2.3 Large eruption dataset

Evidence of the most voluminous eruptions (>0.6 km^3 bulk rock[1]) of Mt Taranaki are found preserved as thick pumice layers within the soil of the surrounding ring plain, mostly to the east of the volcano (Alloway et al. 1995). Many of these were identified and assigned approximate ages by their relative stratigraphic position in relation to radiocarbon dated horizons. Their ages are therefore often approximate, with associated errors spanning ≥200 years (Table 1). Mt. Taranaki sourced tephras are also identified within sediments of lakes of the Waikato district, 200 km NE of the volcano. Due to the distance from source, these units are also likely to be derived from large events. These were precisely dated by Lowe (1988) (Table 1). In addition, we have independently identified the largest Holocene eruptions on the basis of the thickest (>1 cm) and coarsest (mean >250 μm) fall deposits contained within the records of Lakes Umutekai and Rotokare. These units were also correlated by their unique geochemical compositions to large (~1 m thick) pumice deposits within soil sequences on the edifice. This process enabled a much more precise estimate of ages, with smaller and well-defined error ranges typically less than ± 50 years (Table 1). These large-volume explosive eruptions occur on a semi-regular interval of ~400-600 years. Importantly, the majority of them occur during periods of relative quiescence in eruption activity and typically immediately prior to a substantial period of repose, as evidenced by the longest periods of paleosol development in regional stratigraphic profiles.

3. Magmatic evolution of Mt. Taranaki during the Holocene period

3.1 Identifying geochemical trends

Typically whole rock geochemistry, particularly trace element components are used to decipher and model the magma parental sources and subsequent differentiation through ascent (e.g., Price et al. 2005). The tephra deposits collected from the lacustrine and swamp cores of this study are typically less than 55 mm^3, too small to produce consistent whole-sample compositional data, due to variations in the relative abundances of atmospherically sorted phenocrysts. Alternatively, glass composition is also used to provide an indication of the magma composition and inferences on ascent and storage processes (c.f., Shane 2005; Gamble et al. 1999; Andreastuti et al. 2000). At andesite volcanoes, however, glass composition studies often reveal large spreads in data (Shane 2005; Platz et al. 2007). This spread is caused by variable degrees of crystallisation and diffusion processes operating during their ascent and eruption (Blundy et al. 2006), meaning glass will not give an accurate proxy of the true magma composition. A procedure developed by Platz et al. (2007) can be used to estimate the proportions of the main contaminant phase(s) of andesite glass analyses and thus allow back-calculation of glass compositions to more closely estimate those of the melt prior to eruption. However, variations of particle type are also common to andesitic tephras, resulting from the incorporation of material from the conduit walls or lava plug/domes, generating additional composition variation (Platz et al. 2007). Very late stage crystallisation of microlites also leads to strong variations in the surrounding melt on the micro-scale (Best, 2003). In addition, it was found throughout this present study that glass shards from Mt. Taranaki are

[1] Using the method of Legros (2000) on datasets from Alloway et al. (1995).

typically very thin, typically <10 µm, and hence too small for the defocused electron beam used for reliable glass analyses.

Table 2 *Titanomagnetite analyses from each of the identified magma batches. Sample numbers refer to dataset used in this study. M=Maketawa. U=Umutekai. FeO and Fe_2O_3 recalculated (36 oxygens per 24 cations). The titanomagnetite compositions were determined by election microprobe analyses using a JEOL JXA-840 equipped with an energy dispersive spectrometer at the University of Auckland. Analytical conditions include an accelerating voltage of 15kV, a beam current of 600 pA and 100 seconds live time.*

Batch no. (Age ranges yrs B.P.)	**0 (0-1800)**	**1 (1800 - 3000**	**2 (c.3000 - 4600)**	**3 (4600-6000)**	**4 (6000 – 7700)**	**5 7700-c.8600)**	**6 (c8600 – 10 100)**	**7 >10100**	**Fanthams Peak**
Sample no.	**M04-52**	**U05-6**	**U05-19**	**U05-44**	**U05-56**	**U05-72**	**U05-85**	**U05-95**	**U05-8**
Wt%									
SiO_2	0.15	0.15	0.01	0.29	0.2	0.09	0.27	0.15	0.10
TiO_2	6.01	6.94	7.46	8.26	9.69	8.51	9.73	7.76	7.32
Al_2O_3	3.93	3.99	1.94	2.62	2.69	2.98	3.29	3.12	4.40
FeO	32.71	33.29	34.38	35.01	36.00	33.86	35.39	33.91	32.36
Fe_2O_3	53.66	51.48	53.16	52.25	49.95	50.65	47.26	52.85	52.82
MnO	0.41	0.47	1.13	0.97	0.89	0.88	0.65	0.58	0.56
MgO	2.82	2.73	1.8	2.73	2.92	2.85	3.13	2.92	3.28
Total	99.69	99.05	99.88	102.13	102.34	99.83	99.72	101.29	100.75

Ideally, the composition of crystalline phases in equilibrium with a surrounding melt should be used to determine the magmatic evolution of that magma. However, there are many processes that control the composition of the crystallising mineral. For example, variations in pressure, temperature and oxygen fugacity may control the resulting composition (e.g., Hammarstrom and Zen (1986) suggests that abundance of Al_2O_3 within an amphibole crystal is mostly controlled by pressure). In addition, most crystalline phases exhibit solid solutions between distinct end-member compositions and differences in the activation energy at the surface of the crystal may favour the partitioning of one element over another (Ghiorso and Sack 1995). Titanomagnetite, however, is mostly unaffected by these processes because it always exhibits a homogeneous core equilibrated with the magma (Tomiya and Takahashi 2005).

3.2 Titanomagnetite compositions

Titanomagnetite microphenocrysts (~60-100 μm) are abundant in andesitic eruptions and, unlike the typically large phenocrysts of other mineral phases (>150 μm), these microphenocrysts are often incorporated in glass shards that are deposited great distances from the volcano (c.f., Shane 2005). Large elemental diffusion rates in titanomagnetite mean that its composition reflects the composition of the surrounding melt and physical conditions just prior (days to years) to eruption (Devine et al. 2003; Tomiya and Takahashi 2005). In addition to this, the relatively rapidly ascending and quenched magma of sub-plinian, pumice producing eruptions means that the titanomagnetite compositions are unaffected by 'late-stage' crystallisation and chemical differentiation (Burton 1991). Titanomagnetite MgO and Al_2O_3 compositions reflect the relative proportions of these elements within the surrounding melt (Streck et al. 2002). In general, MgO and Al_2O_3 within the melt decrease during continued crystallisation (Hill and Roeder 1974). For example, if extensive plagioclase and/or amphibole are crystallised, then the amount of Al_2O_3 available for subsequent titanomagnetite crystallisation would be relatively low (e.g., Tomiya and Takahashi 2005). In contrast, the abundance of TiO_2 within titanomagnetite is strongly dependent upon oxygen fugacity and temperature of the surrounding melt (Buddington and Lindsely 1964; Devine et al. 2003).

3.3 Titanomagnetite-defined magma batches

The precise age model for the Holocene tephra record of Mt. Taranaki provides the best opportunity to identify changes within magma compositions and thus allow interpretation of the magmatic processes and their timescales. To ensure that between various locations, consistent individual eruption products were used, the STEPDISK procedure (SAS Institute Inc., 2004) was employed to classify correlatives based on their TiO_2, Al_2O_3 and MgO contents within titanomagnetite (Turner et al. in press). Since Al_2O_3 and MgO abundances within the titanomagnetites are closely related to the composition of the magma, whereas TiO_2 is related to oxygen fugacity, bi-variant plots of either Al_2O_3 or MgO vs. TiO_2 can be used to identify clusters of eruptives whose magmatic conditions were similar. On the basis of the age of the eruption, along with its titanomagnetite geochemistry, the Holocene dataset of Mt. Taranaki eruptions was divided into seven compositionally and temporally distinct clusters of data (Fig. 2, ellipsoids labelled 0-6). This implies there were individual parental magmas for each cluster, each with a unique magmatic evolutionary history (Table 2). Here we define these compositionally and temporally classified clusters as magma "batches". Along with the seven batches, an additional highly spread group of high-Al_2O_3 titanomagnetites occurs (black dots on Fig. 2) that overlaps in age with magma batches 0 to 2. Tephras of this group are basaltic-andesite in whole-rock composition and scoriaceous in appearance, which through correlation to near-source sequences, show they were sourced from the basaltic-andesite satellite cone of Fanthams Peak, rather than the summit vent (see Fig. 1). The Fanthams Peak eruptions are therefore grouped separately. Each of seven summit magma batches generated a series of eruptions that was ~1000-2000 years long.

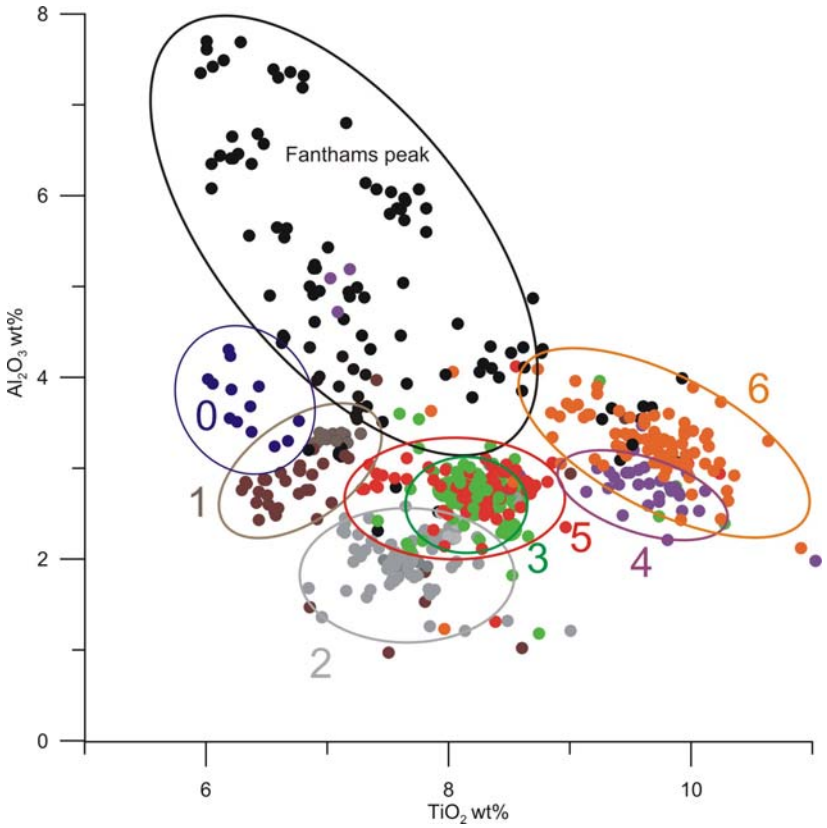

Figure 2: *Plot of electron-microprobe derived Al_2O_3 vs. TiO_2 wt.% in titanomagnetite grains for the entire Holocene record of sub-plinian tephra eruptions from Mt. Taranaki. Each numbered and coloured set of points indicates individual batches of related compositions erupted from the summit vent, which are also temporally constrained (hence the apparent overlaps of some groups). The black dots indicate titanomagnetite derived from more primitive Fanthams Peak eruptions that overlap temporally with summit batches 0 and 1.*

3.4 Magma batches defined by whole-rock geochemistry

Although the tephras within the lacustrine deposits of this study are not suitable for whole-rock geochemical analyses (see above), in Turner et al. (in press) the correlation of tephras to proximal deposits on the volcanic edifice, using titanomagnetite chemistry, was made. The proximal equivalents have clasts large enough for more representative whole-rock geochemical analysis. Fresh dense juvenile and pumice clasts were individually selected for analysis (Table 3).

Table 3 *Representative whole rock geochemical samples. Major and trace element concentrations were measured by X-ray fluorescence (Siemens SRS303AS spectrometer) using standard techniques on glass fusion discs prepared with SPECTRACHEM 12-22 (lithium tetraborate/lithium metaborate) flux following the method of Norrish and Hutton (1969). Major elements have one-sigma relative errors <1%, whereas trace elements have one-sigma relative errors of <1% for Sr and Zr, 1-3% for V, Cr, Cu, Zn, Ga and Y, 3-5% for Sc and Ni and 5-10% for Rb and Nb. In addition Cs, Ba, Pb, Th, U, Hf, Ta, and Rare Earth Elements (REE) were analysed by LA-ICP-MS at the Research School of Earth Sciences, Australian National University, using an Excimer LPX120 laser and Agilent 7500 series mass spectrometer. For this work the same fused glass discs as for XRF were used. Detection limits are <1 ppb and analytical errors <1% relative.*

Sample no.	**M04-52**	**M04-57**	**E02-84**	**E02-173**	**M04-80**	**M04-90**	**M04-166L**	**M04-176L**
Age (yrs B.P.)	**300**	**500-800**	**1900**	**1800**	**3600**	**3600**	**4600**	**4800**
Batch no.	**0.00**	**0.00**	**1.00**	**1.00**	**2.00**	**2.00**	**3.00**	**3.00**
Wt%								
SiO_2	55.30	55.51	53.34	53.56	56.96	57.95	55.14	54.42
TiO_2	0.77	0.81	0.84	0.86	0.60	0.60	0.82	0.83
Al_2O_3	17.14	18.04	17.69	17.35	18.55	18.13	18.04	18.11
Fe_2O_3	7.21	6.91	8.21	8.18	5.74	5.73	7.49	7.59
MnO	0.15	0.15	0.17	0.17	0.17	0.17	0.16	0.16
MgO	3.56	2.40	3.40	3.71	1.67	1.70	2.77	2.62
CaO	7.85	6.68	8.18	8.55	6.69	6.67	8.04	7.71
Na_2O	3.62	3.91	3.59	3.61	3.99	4.10	3.80	3.67
K_2O	2.63	2.74	2.02	2.09	2.21	2.32	2.19	2.14
P_2O_5	0.27	0.33	0.28	0.27	0.29	0.29	0.29	0.29
H_2O	0.17	0.45	0.44	0.21	0.78	0.51	0.37	0.49
LOI	0.71	1.64	1.26	0.78	1.63	1.16	0.13	0.55
Total	99.37	99.58	99.41	99.35	99.28	99.32	99.24	98.58
ppm								
Sc	20.00	15.00	15.00	22.00	5.70	5.30	10.00	11.50
V	202.00	185.00	210.00	219.00	105.90	108.60	203.50	204.90
Cr	41.00	4.00	23.00	37.00	16.40	8.40	23.00	12.50
Ni	10.00	0.00	4.00	4.00	3.20	0.00	6.70	6.60
Cu	92.00	84.00	66.00	83.00	23.10	59.40	18.70	82.30
Zn	81.00	83.00	87.00	88.00	76.80	99.20	80.20	96.40
Ga	23.00	24.00	19.00	19.00	21.20	19.00	21.20	21.40
Rb	67.00	70.00	51.00	52.00	56.00	55.80	59.60	58.60
Sr	583.00	692.00	628.00	630.00	673.20	647.00	662.00	647.20
Y	22.00	24.00	23.00	23.00	24.00	24.50	24.30	24.80
Zr	134.00	153.00	127.00	118.00	143.40	139.90	134.20	135.10

Nb	5.16	6.18	4.65	4.46	5.11	5.05	4.62	4.55
Cs	3.92	3.74	2.75	2.75	3.56	3.77	2.96	3.51
Ba	972.32	1037.04	720.25	753.13	899.44	911.76	777.15	770.43
La	20.51	22.79	15.21	17.57	21.75	21.53	16.56	20.04
Ce	38.72	43.98	31.17	32.12	42.69	42.04	33.71	35.89
Pr	4.84	5.46	4.00	4.18	5.25	5.33	4.36	4.70
Nd	20.28	23.30	18.13	18.61	22.29	22.70	19.62	20.72
Sm	4.62	5.16	4.12	4.33	4.91	4.87	4.49	4.54
Eu	1.27	1.34	1.22	1.27	1.25	1.35	1.35	1.40
Gd	4.12	4.79	4.12	4.39	4.45	4.53	4.30	4.58
Tb	0.69	0.73	0.67	0.71	0.71	0.72	0.69	0.76
Dy	3.95	4.11	3.75	3.78	4.04	4.14	3.93	4.32
Ho	0.78	0.81	0.78	0.81	0.83	0.86	0.87	0.89
Er	2.23	2.28	2.19	2.31	2.54	2.49	2.40	2.48
Tm	0.30	0.31	0.28	0.31	0.33	0.32	0.28	0.32
Yb	2.16	2.26	2.01	2.11	2.42	2.36	2.17	2.33
Lu	0.33	0.36	0.30	0.32	0.36	0.37	0.38	0.37
Hf	4.22	4.60	3.44	3.24	3.97	4.04	3.86	3.90
Ta	0.73	0.79	0.38	0.40	0.40	0.45	0.39	0.38
Pb	13.46	13.87	10.87	10.17	14.87	14.63	10.68	11.23
Th	8.57	9.06	6.27	5.87	8.74	8.32	6.45	6.24
U	2.04	1.97	1.33	1.30	2.00	1.92	1.47	1.43

Table 3 (continued)

Sample no.	M05-74	M05-75	M05-78	M05-78L	M04-100	M04-102	E03-61	EB-4b
Age	**7068**	**7700**	**7939**	**7939**	**8917**	**9347**	**1700**	**1700**
Batch no.	**4.00**	**4.00**	**5.00**	**5.00**	**6.00**	**6.00**	**Fanthams**	**Fanathams**
Wt%								
SiO_2	54.54	55.55	53.75	54.53	54.20	54.68	50.93	51.08
TiO_2	0.89	0.83	0.75	0.75	0.88	0.89	1.06	1.01
Al_2O_3	18.96	19.22	19.07	17.88	18.54	18.34	17.75	17.36
Fe_2O_3	7.79	7.19	7.42	7.47	7.75	7.60	9.90	9.63
MnO	0.17	0.17	0.17	0.17	0.17	0.16	0.18	0.17
MgO	2.60	2.48	2.47	2.64	2.64	2.70	4.27	4.56
CaO	7.87	7.65	7.59	7.69	8.28	8.16	9.74	9.44
Na_2O	3.65	3.74	3.59	3.69	3.94	3.89	3.43	3.37
K_2O	2.09	2.10	1.95	2.11	2.04	2.17	1.84	1.84
P_2O_5	0.33	0.31	0.32	0.29	0.31	0.30	0.28	0.27
H_2O	0.25	0.00	0.56	0.82	0.31	0.27	0.06	0.05
LOI	0.30	0.28	1.91	1.64	0.66	0.58	-0.04	0.52
Total	99.44	99.52	99.54	99.67	99.73	99.74	99.39	99.32
ppm								
Sc	12.00	14.00	9.00	10.00	10.00	12.20	22.00	25.00
V	190.00	164.00	161.00	174.00	197.40	203.40	297.00	277.00
Cr	0.00	22.00	3.00	6.00	11.60	10.10	20.00	41.00
Ni	0.00	7.00	2.00	2.00	3.10	4.10	8.00	12.00
Cu	50.00	40.00	55.00	23.00	75.00	73.00	113.00	100.00
Zn	94.00	96.00	86.00	92.00	82.40	74.00	89.00	84.00
Ga	25.00	25.00	25.00	24.00	22.20	21.90	19.00	19.00
Rb	52.00	53.00	48.00	52.00	50.50	51.70	44.00	43.00
Sr	634.00	671.00	686.00	672.00	722.90	710.40	620.00	597.00
Y	26.00	27.00	23.00	22.00	25.00	24.70	23.00	21.00
Zr	140.00	148.00	127.00	119.00	132.30	127.40	106.00	105.00
Nb	5.17	5.64	5.27	4.88	4.94	4.49	3.87	3.90
Cs	3.02	3.22	3.00	2.68	2.92	2.97	2.25	2.23
Ba	760.74	778.43	763.47	804.29	735.08	756.41	666.37	671.87
La	18.37	18.76	19.51	15.61	19.60	17.64	13.46	15.42
Ce	36.45	38.35	34.29	30.88	37.95	35.50	28.83	27.45
Pr	5.06	5.22	4.36	3.98	4.95	4.68	3.79	3.67
Nd	22.18	22.77	19.36	17.68	21.90	21.04	17.42	16.96
Sm	4.95	5.15	4.37	4.11	5.13	4.90	4.48	4.08

Eu	1.46	1.45	1.31	1.30	1.43	1.41	1.30	1.27
Gd	5.25	4.92	4.14	3.86	4.93	4.88	4.11	4.14
Tb	0.83	0.82	0.68	0.65	0.79	0.75	0.70	0.66
Dy	4.50	4.56	3.88	3.62	4.16	4.14	3.81	3.69
Ho	0.97	0.98	0.78	0.76	0.87	0.86	0.78	0.74
Er	2.68	2.76	2.28	2.17	2.44	2.37	2.21	2.14
Tm	0.34	0.36	0.31	0.28	0.32	0.31	0.29	0.29
Yb	2.51	2.45	2.18	1.98	2.26	2.26	1.95	1.96
Lu	0.38	0.37	0.34	0.31	0.34	0.35	0.28	0.28
Hf	4.35	4.37	3.72	3.53	3.77	3.60	2.93	2.83
Ta	0.55	0.39	0.50	0.37	0.37	0.36	0.27	0.33
Pb	12.47	13.35	13.63	11.64	11.54	11.67	4.66	4.97
Th	7.01	7.34	6.77	6.12	6.06	5.79	4.45	4.53
U	1.48	1.54	1.59	1.46	1.35	1.35	1.06	1.08

The whole-rock major and trace element data of these dated tephras also clearly group the eruptive record into compositional and temporal 1500-2000 year batches, identical to those from the titanomagnetite chemistry (Fig. 3). This is also consistent with the conclusions of Downey et al. (1994) who identified probable ages of four lava-flow groups on Mt. Taranaki and suggested that each was emplaced during eruption cycles lasting 1000-2000 years. Although these lava-flow groups are not precisely dated, contrasting geochemical variations between these different stratigraphic groups (Price et al. 1999) are consistent with the trace element data presented here (Fig. 3).

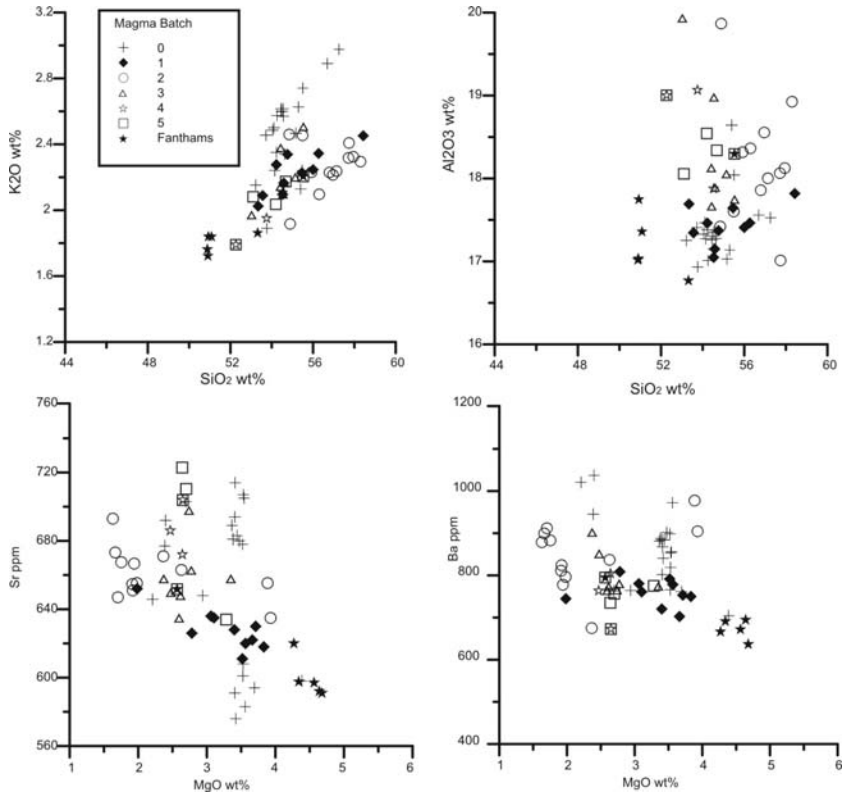

Figure 3: *SiO_2 and MgO variation diagrams for Taranaki eruptives. These data also cluster into defined "batches" that correlate to those defined on the basis of titanomagnetite chemistry.*

3.5 Geochemical magma cycles

The MgO content of titanomagnetite microphenocrysts can be used to approximate the overall composition of the magma from which they were crystallised. Hence they provide an opportunity to identify changes and/or trends within the evolution of Mt. Taranaki's magmatic system throughout the Holocene (Fig. 4). A regular fluctuation between primitive and relatively evolved end members is apparent, with a periodicity of between 1000 to 2000 years. The compositional trend from Fanthams Peak also displays a gradual decrease in MgO content from its initial eruption 3000 years ago, through to its last observed eruption approximately 1500 years B.P. Therefore, the magma batches feeding Fanthams Peak eruptions also follow a similar compositional evolution trend as that observed for the summit magmas (Fig. 4). With the exception of the partly overlapping geochemical trends between batches 2 to 3, each peak in eruption frequency corresponds with rise of an individual magma batch. This shows a strong relationship between the mid-point of a magma batch's existence and the highest eruption frequency. During the period in which batches 2 and 3 erupted, the geochemistry of individual tephras indicates that eruptions were at times tapping both magma batches more or less concurrently.

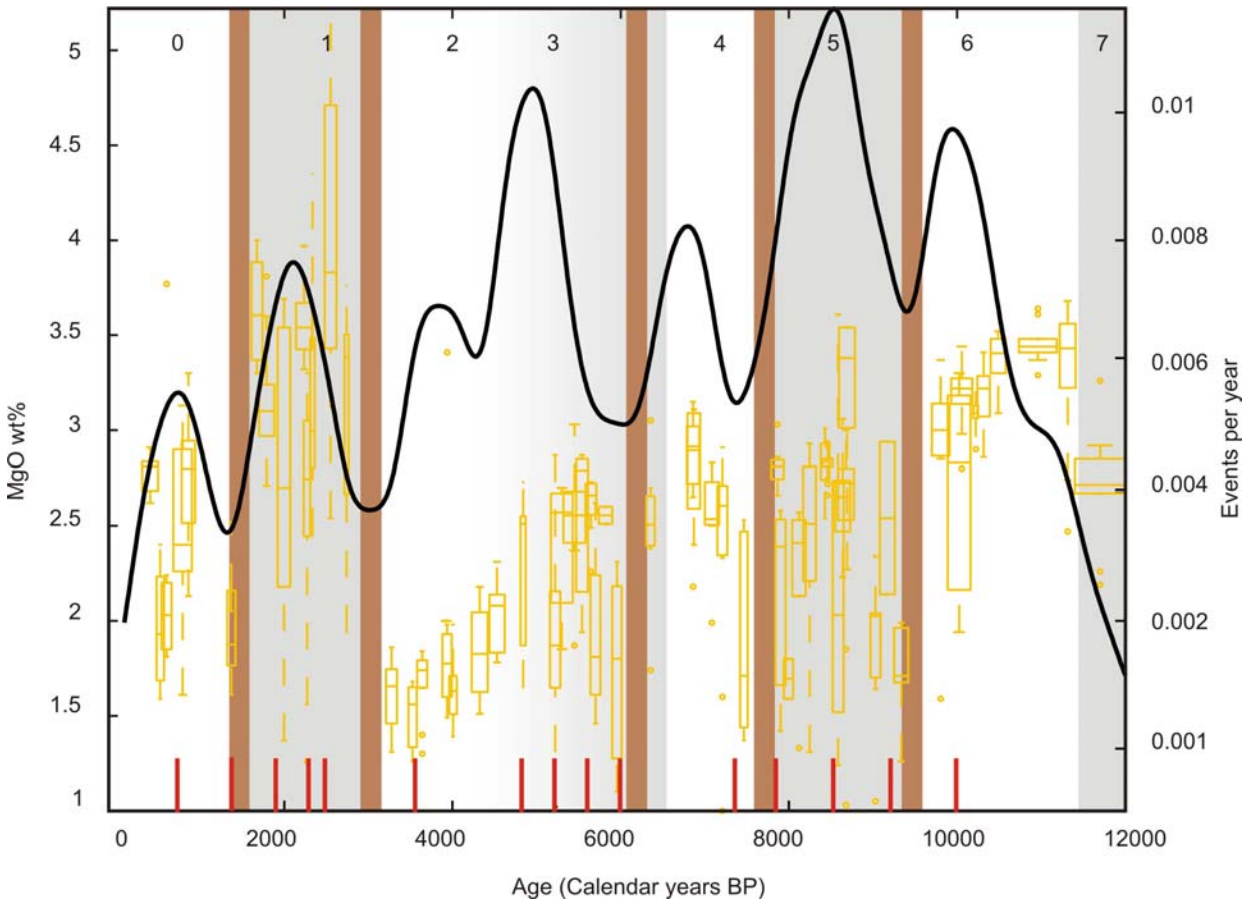

Figure 4: *Black curve shows the rate of sub-Plinian (pumice) eruptions (left Y-axis). Orange box and whiskers plots represent the ranges of MgO concentrations in titanomagnetite crystals within erupted products. Timing of recharged eruption events are shown at the base of the plot in red – identified bi-modal titanomagnetite populations within the erupted deposits. Individual magma batches are vertically shaded alternately white and grey. Periods of intense soil development (indicating quiescence) from on-volcano sites are indicated by vertical brown shaded zones.*

4. Implications for probabilistic eruption forecasting

Turner et al. (2008a) showed that there was no relationship between the repose period preceding an eruption from Mt. Taranaki and its size. However, this previous study neglected large eruptions that were not directed towards Lake Umutekai. Using a more complete dataset of the largest tephras identified by both Alloway et al. (1995) and in this study (Tables 1), suggests that the largest eruptions precede the longest periods of repose.

The last recorded eruption from Mt. Taranaki was at least 150 years ago (Platz 2007) and this was relatively minor (i.e., dome growth activity). At present an organic-rich soil is developing on edifice stratigraphic profiles. This demonstrates that we are clearly within a period of repose. The Burrell eruption (300 ± 60 yrs B.P.; Fergusson and Rafter 1957) was the latest large eruption from Mt. Taranaki and the largest over the past 1500 years. Like the other large eruptions, it was erupted prior to an extended period of repose. The highly evolved compositions of the magma involved in this eruption compared to the previous event in the series indicates that the volcano may be about to erupt a new magma batch (Fig. 4).

Although we can simplify the geochemical trend for the volcano into c. 1500 year magma batches with repeating evolutionary cycles, the magmatic system is likely to be far more complex, with the magma of individual eruptions also being affected by late-stage magma mixing, assimilation, and crystal fractionation processes (Price et al. 2005; Annen et al. 2006). Evidence of this at Mt. Taranaki can be observed within the complex geochemical trends during eruptions of magma batches 2 and 3 (4000-5000 yrs B.P.). In addition, the geochemistry of the Korito Tephra (4150 ± 100 yrs B.P.; Alloway et al. 1995) is much more evolved than the titanomagnetite geochemical trend suggests (Fig. 4). The Korito Tephra may therefore also be an “end of cycle” eruption.

5. Mechanisms for magma generation at andesite volcanoes

5.1 Models of andesite magma generation

Geochemical evidence from titanomagnetite and whole-rock datasets of Mt. Taranaki eruptives were used to identify geochemically and temporally distinct magma batches. Each magma batch has a history of around 1500-2000 years of eruptions and geochemical evolution, from relatively mafic to increasingly silicic compositions.

Traditional models (Fig. 5A) of andesitic magma differentiation involve crystal-fractionation and assimilation (AFC) of mantle derived basaltic or basaltic-andesite magma in shallow crustal chambers (Sisson and Grove 1993; Grove et al. 1997). For example, fractional crystallisation of H_2O-saturated basalts and basaltic-andesites at andesitic temperatures (950-1050°C) by crystallizing plagioclase (An_{60-90}) + clinopyroxene + amphibole + oxides ± orthopyroxene ± olivine can generate an andesitic magma (Sisson and Grove 1993; Grove et al. 1997). However, differentiation of basaltic magma within the upper crust would result in abundant, dense, complementary mafic cumulates and these do not occur within the shallow crust (Glazner, 1994). To overcome the problems of the missing mafic cumulates, recent research has focused on similar

fractionation processes. Instead of taking place within upper crustal zones, these processes occur at or close to the Moho (Annen and Sparks 2002; Mortazavi and Sparks 2004; Prouteau and Scaillet 2003). Primitive basaltic magmas that have a wide range of compositions are produced by partial melting of harzburgite in the mantle wedge, fluxed by either a combination of H_2O-rich fluids liberated from the subducting slab (Tatsumi 1982; Grove et al. 2002; Carmichael 2002), or decompression melting resulting from mantle flow (McKenzie 1985). The characteristically high-Mg magmas are subsequently intruded into the upper mantle/lower crust. Numerous intrusions of this material accumulate within the lower crust and raise the geotherm, resulting in the development of an environment suitable for new magma generation (Fig. 5B). This zone is here termed the "lower crustal hot-zone" (c.f., Annen et al. 2006). Silicic and intermediate magmas are generated by 1) incomplete crystallisation of basaltic material (Annen and Sparks 2002; Prouteau and Scalillet 2003); 2) the dehydration partial melting of earlier, partly crystallised basalt intrusions and/or meta-basalts (amphibolite) by the intrusion of new hot mantle-derived magma (Smith and Leeman, 1987; Annen and Sparks 2002; Price et al. 2005); and 3) crustal assimilation (DePaolo et al. 1981; 1992). The gradients of temperature, pressure and water contents within the lower crust control the rate of melt production, which ultimately controls the composition of the melt that segregates and rises to upper crustal areas. These magmas are intruded to the limit of "neutral buoyancy" based on their density in relation to host rock (Jackson et al. 2003). As the ponded magma thickens, density-stratified layers begin to form (i.e., when differences in density exceed c. 100 kg m^{-3}; Dufek and Bergantz 2005), driven by differences between areas of local cooling vs. areas affected by a semi-continuous influx of new material from the mantle. The boundary between each layer may not be well defined, and mixing between layers of different degrees of evolution may occur. Hence the entire zone could be conceptualised as a stratified crystal mush (similar to that described in Couch et al. 2003).

5.2 Magma recharge models

Mt. Taranaki eruptives have a typically complex phenocryst assemblage that indicates equally complex magmatic evolution processes, including magma mixing (Heiken and Eichelberger 1980), entrainment of old crystals from previously consolidated magmas (Davidson et al. 2005), crystal growth through degassing (Blundy and Cashman 2001) and some degree of amalgamation of magma bodies derived from many previous episodes of ascent (Turner et al. 2008c).

In Turner et al. (2008c) it was shown that the zoning profiles of plagioclase, clinopyroxene and amphibole rims suggest that Taranaki magmas have undergone a number of 'recharges' with influxes of new magmas that were only slightly hotter and richer in H_2O than the resident bodies. Compositional data from titanomagnetite microphenocrysts from many Holocene eruptions in this study, compiled for correlation purposes in Turner et al. (in press), indicate that bi-modal populations are common in many Holocene units (Fig. 4), and are clearly represented in their TiO_2-contents. Bimodality in this case indicates magmas that have erupted soon after recharge, without time for the resident titanomagnetites to re-equilibrate (Turner et al. 2008c). Here titanomagnetites are used to indicate recharge events in the temporal record (although other recharged magmas may be missing from this record, if the recharge event occurred some decades before eruption). The recognised recharge events occur periodically, separated by irregular intervals of 400-500 years. They are evidently no more intense during high-frequency periods of eruption, nor are they concentrated in the early phases of a geochemical cycle. This implies that

such recharge events occur independently of the magma batches recognised earlier and therefore reflect some other magma segregation process occurring at depth.

The Holocene geochemical trends observed at Mt. Taranaki can result from either:

1) multiple recharges to an upper-level magma system throughout the geochemical cycle. In this case magma differentiation occurs at depth and recharge events bring up sequentially more evolved magma until a new magma batch is tapped (Fig. 5A), or

2) due to a complex interplay of different magma at various levels within the upper crustal system (i.e., Price et al. 2005), recharged magma may mingle and mix with other bodies of magma resulting in 'recharge' signatures within many eruptions shortly following the intrusion of new magma from depth (Fig. 5B).

As indicated above, the compositional changes during the eruption of a defined magma batch appear to be more closely related with the pattern of eruption frequency of Mt Taranaki (Fig. 4). This must relate to another process occurring at depth where each batch is produced, and subsequently evolved.

5.3 Magma segregation

The segregation of a buoyant, partial melt and its crystal cargo from a single layer within the deep crustal hot zone can result from a number of mechanisms. Compaction-induced magma segregation may occur if continued intrusion and emplacement of mantle-derived basalts into the zone occurs, increasing local pressures (e.g., McKenzie 1985). In this case, melt segregation produces porosity waves which move buoyantly upwards (Jackson et al. 2003). Mantle-derived basalts have densities of over 2600 ± 100 kg m^{-3}, depending primarily on their water contents (McKenzie 1985). During subsequent AFC processes, magma densities can also be significantly altered, producing buoyancy instability and porosity waves (Jackson et al. 2003). Once the melt is segregated, magma will continue to move upwards and accumulate at depths just above the solidus (Jackson et al. 2003; Annen et al. 2006), or where it encounters crustal rocks that are considerably less dense and thus impermeable.

At Taranaki, the regional basement crustal rocks belong to the Median Tectonic Zone; a series of plutonic/volcanic and ultramafic rocks of Cretaceous age (Mortimer et al. 1997). These rocks are abutted by greywacke, which is geophysically constrained as occurring at 7-12 km depth (Sherburn et al. 2006). Greywacke, the lowest density of basement rocks, at 2700 kg m^{-3} is denser than andesitic melts of 2555 kg m^{-3}; (Platz 2007), 2680 ± 150 kg m^{-3} (Hunt and Woodward 1971), and 2640 ± 100 kg m^{-3} (Locke and Cassidy 1997). Magma should therefore easily pass through these basement rocks. Pleistocene to Eocene sandstones and mudstones are the dominant rock strata above 6 km depth (Sherburn et al. 2006), with densities increasing with depth/age from 2200 kg m^{-3} to 2600 kg m^{-3} (Hatherton and Leopard 1964). Andesitic melts segregated from the lower crust will rise to a maximum depth of c. 7 km before stalling in these lower-density materials. Basaltic-andesites of the Fanthams Peak suite probably stalled at slightly lower levels (6-10 km) because their densities are similar to that of greywacke (Platz 2007). The geophysically identified brittle-ductile transition at approximately 10-7 km also independently constrains the upper limit of magma assembly beneath Mt. Taranaki (Sherburn and White 2006).

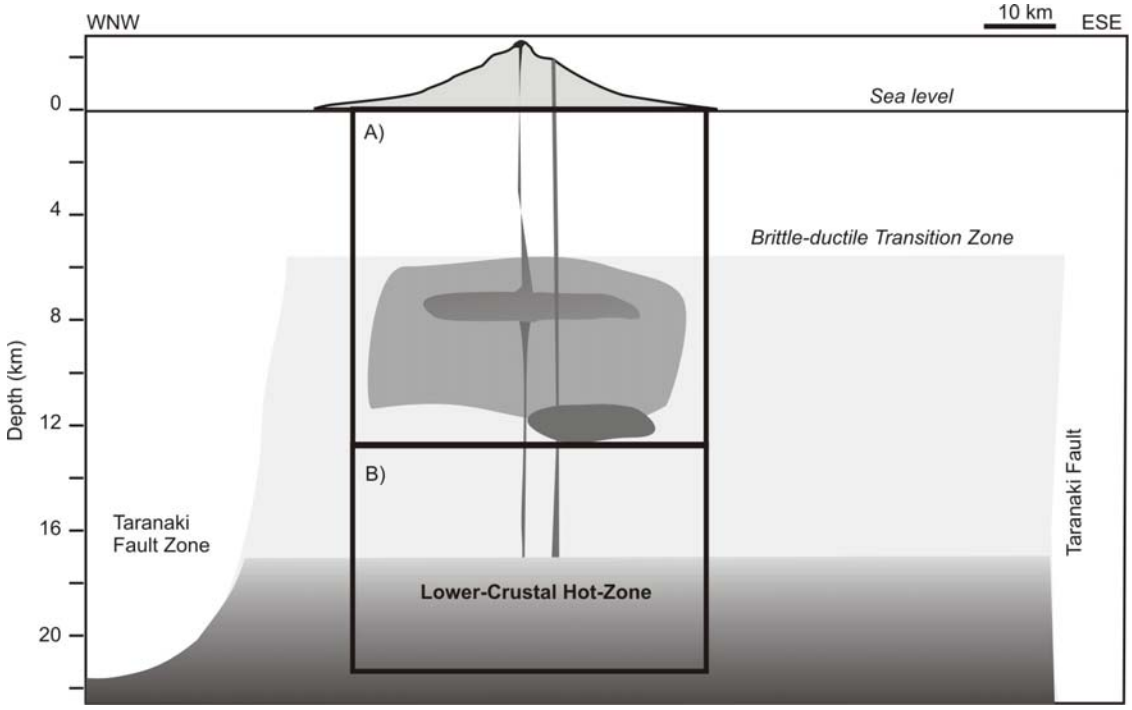

Figure 5: *Conceptual model of the magmatic system of Mt. Taranaki. A) Traditional AFC magma body model, where a 'False' recharge signature is given by magma mingling within the upper magma system, convection or reheating during conduit processes through to ascent. B) Magma differentiation occurs at depth within the lower crustal hot-zone with single magma batches feeding the upper magma system for approximately 1500 years. The recharge events of the upper system from the hot-zone occur periodically but irregularly throughout the record, separated by intervals of <400-500 years. Depth estimates from Grunder (2006) and geophysical constraints from Sherburn and White (2005)*

5.4 Structural consequences of magma assembly

Increased pressurisation and the onset of magma ascent and eruption may be driven by continued degassing and crystallisation of a magma body within the upper magma system. Pressurisation resulting from the input of new magma and/or crystallisation of existing magma, generates low-magnitude earthquake swarms as the surrounding country rock adjusts (Gerst and Savage 2004). An example of this are the earthquake swarms that occurred during the 1995-1996 eruptions of Mt. Ruapehu, up to 20 km SE of the volcano (Hayes et al. 2004). Earthquake swarms on the Cape-Egmont Fault Zone, 15-20 km west of Mt. Taranaki, are inferred to be the result of changing pressures in the magmatic system (Sherburn and White 2006).

The N-S orientation of the Holocene vents of Mt. Taranaki provides an indication of the orientation of the conduit dike system (Sherburn and White 2006). Magma intrusion into this system would result in a local stress field that would be east-west compressive, consistent with that currently observed in earthquake swarms of the Cape-Egmont Fault Zone (Sherburn and White 2006). In Taranaki there are two recently active fault structures, the Inglewood and Oaonui Faults (Fig. 1). Like many of the faults within the Taranaki district, these have a northeast-

southwest orientation, relating to their initial formation during a continental rifting event that separated New Zealand from Australia at around 80 Ma (King and Thrasher 1996). Therefore their orientation no longer reflects the current stress field (Sherburn and White 2006). Oblique-normal movements are characteristic of the intermittent movements on these faults (Sherburn and White 2006), which is in contrast to the current, local east-west compressive stress of western Taranaki. The last major movement on the Oaonui Fault occurred at approximately 6500 yrs B.P. (Hull and Dellow 1993) and for the Inglewood Fault 3300-3500 yrs B.P. (Sherburn and White 2006). These movements are coincident with two of the largest eruptions from Mt. Taranaki during the Holocene:

1) Tephra 63 of the Umutekai core (bulk-rock erupted volume[2] of 0.65 km^3 at 6219 ± 49 yrs B.P.). This tephra is likely to be a correlative of one of the Kaponga Tephra members described by Alloway et al. (1995) and the E-8 ash deposit of Lowe (1988); and

2) Tephra 25 of the Umutekai core correlates with the 3750 yrs B.P. Inglewood eruption (Alloway et al. 1995). This is the largest Holocene eruption from Mt. Taranaki, with a bulk-rock volume of 1.17 km^3.

Sherburn and White (2006) consider that pressurisation of the 6-10 km magmatic system causes fracturing of the surrounding rock. During eruption, release of the local east-west compressive stress induced normal faulting.

5.5 Speculation on eruption frequency and magmatic processes

The geochemical record of Mt. Taranaki shows broad 1500-2000 year long cycles from mafic through to evolved magmas that represent individual magma batches. Some magma batches, such as 5 and 6, are well defined (Fig. 4); however others, such as 2 and 3, are not so distinct. The eruption frequency curve is also more irregular during the eruption of magma batches 2 and 3 (Fig. 4). This appears to be the result of an overlap in timing of production of these two batches, and also their semi-contemporaneous rise and eruption.

From c. 3000 yrs B.P., eruption of a relatively mafic magma batch began from the satellite vent of Fanthams Peak. This followed the last major movement of the Inglewood Fault. Eruption of basaltic-andesite from Mt. Taranaki is not restricted to the last 3000 years of activity and has been identified in rare individual, older lava flows on the edifice (Price et al. 1999) and within the clasts of debris-flows from proto-Taranaki cones (Price et al. 1999; Zernack et al. 2006). However, the basalts and basaltic-andesites of the older record have a much greater mantle component and are lower in K_2O relative to SiO_2 (Price et al. 1999). In addition, samples from the older record (for example Sample T90/42A; Table 2 in Price et al. 1999) have relatively high MgO (6.75 wt%), Ni (119 ppm) and Cr (113 ppm) abundances, suggestive of lower degree melts of the mantle source and subsequently lesser-degrees of fractionation during ascent and eruption (Price et al. 1999).

The trace element geochemistry from the summit and Fanthams Peak magmas between 3000 to 1500 yrs B.P. are virtually identical, which suggests that the two magmas were derived from a

[2] Estimated volume using the single isopleths method of Legros (2000)

similar or single source. This observation is consistent with the concept of the developing lower crustal hot zone. The zone is continually heated as long as mantle-derived basalt continues to be injected. As the whole system is heated, the generation of more-mafic melts may begin. The Fanthams Peak magmas may hence represent melts from a hotter area within the same layer, which is concurrently producing siliceous magmas erupting at the summit. By contrast, the basaltic andesites of the early Taranaki record represent more primitive melts that have passed through the lower crust with little interaction during the early stages of hot-zone development.

6 Conclusions

A precisely dated Holocene record of eruption activity from Mt. Taranaki, New Zealand, has provided an unprecedented opportunity to examine the magmatic driving forces behind variations in eruption frequency at andesitic volcanoes. Highly cyclic eruption frequency was identified at this volcano, with a periodicity of 1500-2000 years. This is matched by geochemical indicators of regular repeating cycles of magma supply, as reflected in titanomagnetite mineral. Each of the ~1500 year periods corresponds to the eruption of a single, geochemically distinct magma 'batch'. Onset of each magma batch is represented by an initial eruption of relatively mafic magma followed by progressively more siliceous eruption products. Each batch culminates in the largest known explosive pyroclastic eruptions from this centre (>0.6 km^3 magma), typically before an extended period of repose. Currently, Mt. Taranaki appears to be within a period of repose, following the latest large explosive eruption occurring at AD 1655. Based on extrapolation of Holocene trends, the next eruptions of Mt. Taranaki should coincide with the onset of a new magma batch.

The primary cause of geochemical variations in Mt. Taranaki magmas is either variation in the degree of amphibole fractionation, and/or the breakdown of pre-existing amphibolite/gabbro assemblages within a 'lower-crustal hot zone'. The model is consistent with the geophysical evidence of Sherburn and White (2005) in which a rise of the brittle-ductile transition from the lower crust (~25 km) to approximately 10 km depth beneath Mt. Taranaki is identified. This suggests that a zone containing partial melts extends between these two depths.

The 1500-2000 year periodicity of magma batches erupted at Mt. Taranaki agrees with the Annen et al. (2006) model, where individual melt-crystal magma batches are formed at depth and subsequently rise to upper crustal magma storage areas. The record of Holocene eruptions that show direct evidence of recharge (represented by bi-modal titanomagnetite chemistry) suggests that rises occur at regular intervals of <400-500 years. These recharge events, however, do not appear to be the controlling factor in eruption frequency of this volcano. Instead the 1500-2000 year geochemical cycle of each magma batch appears to control the overall eruption rate of Mt. Taranaki.

7. Acknowledgements

This study was supported by the NZ FRST contract MAUX0401 and the Earthquake Commission of New Zealand (EQC) Time Varying Hazard Fund. We thank Mr and Mrs Rumball for access to Lake Umutekai and Dr Ritchie Sims (Auckland University) for analytical assistance.

References

Alloway BV, Neall VE, Vucetich CG (1995) Late Quaternary (post 28,000 year BP) tephrostratigraphy of northeast and central Taranaki, New Zealand. J R Soc NZ 25: 385-458.

Andreastuti SD, Alloway BV, Smith IEM (2000) A detailed tephrostratigraphic framework at Merapi volcano, central Java, Indonesia: implications for eruption predictions and hazard assessment. J Volc Geotherm Res 100: 51-67.

Annen C, Sparks RSJ (2002) Effects of repetitive emplacement of basaltic intrusions on thermal evolution and melt generation in the crust. Earth Planet Sci Letters 203: 937–955.

Annen C, Blundy JD, Sparks RJS, (2006) The Genesis of Intermediate and Silici Magma in Deep Crustal Hot Zones. J Petrol 47: 505-539.

Best MG (2003) Igneous and metamorphic petrology. Blackwell Science. Malden.

Blundy J, Cashman K (2001) Ascent-driven crystallisation of dacite magmas at Mount St Helens, 1980–1986. Cont Mineral Petrol 140: 631–650.

Blundy J, Cashman K, Humpreys M (2006) Magma heating by decompression-driven crystallization beneath andesite volcanoes. Nature 443: 76-80.

Buddington AF, Lindsley DH (1964) Iron-titanium oxide minerals and synthetic equivalents. J Petrol 5: 310–357.

Burton BP (1991) The interplay of chemical and magnetic ordering, in Lindsley DH (ed) Oxide minerals: Petrologic and magnetic significance: Washington, District of Colombia. Min Soc Am, pp, 303–321.

Carey S, Sigurdsson H (1985) The May 18, 1980 eruption of Mt. St Helens II: Modeling of dynamics of the Plinian phase. J Geophys Res 90: 2948-2958.

Carmichael ISE (2002) The andesite aqueduct: perspectives on the evolution of intermediate magmatism in west–central (105–99°W) Mexico Contrib Minera. Petrol 143: 641–663.

Cashman KV, Taggart JE (1983) Petrologic monitoring of 1981-1982 eruptive products from Mount St. Helens, Washington. Science 221: 1385-1387.

Chesner CA, Pose WI, Deino A, Drake R, Westgate JA (1991) Eruptive history of Earth's largest Quaternary caldera (Toba, Indonesia) clarified. Geology 19: 200–203, doi: 10.1130/0091-7613(1991)019<0200:EHOESL>2.3.CO;2.

Costa F, Chakraborty S, Dohmen R (2003) Diffusion coupling between trace and major elements and a model for calculation of magma residence times using plagioclase. Geochim Cosmochim Acta 67: 2189–2200.

Condomine M, Gauthier PJ, Sigmarsson O (2003) Timescales of magma chamber processes and dating of young volcanic rocks. In Bourdon B, Henderson G, Lundstrom C, Turner S (Eds.) Uranium Series Geochemistry. Rev Mineral Geochem 52: 125-169.

Couch S, Harford CL, Sparks RSJ, Carroll MR (2003) Experimental constraints on the conditions of formation of highly calcic plagioclase microlites at the Soufrière Hills Volcano, Montserrat. J Petrol 44: 1455–1475.

Davidson JP, Hora JM, Garrison JM, Dungan MA (2005) Crustal forensics in arc magmas. J. Volcanol. Geotherm. Res. 140:157–170.

DePaolo DJ (1981) Trace-element and isotopic effects of combined wallrock assimilation and fractional crystallisation. Earth Planet. Sci. Letters 53:189–202.

DePaolo DJ, Perry FV, Baldridge WS (1992) Crustal versus mantle sources of granitic magmas—a 2-parameter model based on Nd isotopic studies. Transactions of the Royal Society of Edinburgh, Earth Sci. 83: 439–446.

Devine JD, Rutherford MJ, Norton GE, Young SR (2003) Magma storage region processes inferred from geochemistry of Fe-Ti oxides in andesitic magma, Soufriere Hills Volcano, Montserrat, WI. J Petrol 44: 1375-1400 (DOI:10.1093/petrology/44.8.1375).

Downey WS, Kellett RJ, Smith IEM, Price RC, Stewart RB (1994) New paleomagnetic evidence for the recent eruptive activity of Mt. Taranaki, New Zealand. J Volcanol Geotherm Res 60: 15-27.

Druce AP (1966) Tree ring dating of recent volcanic ash and lapilli, Mt. Egmont. NZ J Bot 4: 3-41.

Dufek J, Bergantz GW (2005) Lower Crustal Magma Genesis and Preservation: a Stochastic Framework for the Evaluation of Basalt–Crust Interaction J Petrol 46: 2167-2195.

Fergusson GJ, Rafter TA (1957) New Zealand C14 measurements – 3. NZ J Sci Technol B38: 732–749.

Gamble JA, Wood CP, Price RC, Smith IEM, Stewart RB, Waight T (1999). A fifty year perspective of magmatic evolution on Ruapehu Volcano, New Zealand: verification of open system behaviour in an arc volcano. Earth and Planet Sci Lett 170: 301–314.

Gerst A, Savage MK (2004) Seismic anisotropy beneath Ruapehu Volcano: a possible eruption forecasting tool. Science 306: 1543-1547

Ghiorso MS, Sack RO (1995) Chemical mass transfer in magmatic processes IV. A revised and internally consistent thermodynamic model for the interpretation and extrapolation of liquid–solid equilibria in magmatic systems at elevated temperatures and pressures. Contrib Mineral Pet 119: 197–212.

Glazner AF (1994) Foundering of mafic plutons and density stratification of continental crust. Geology 22: 435–438.

Grove TL, Donnelly-Nolan JM, Housh T (1997) Magmatic processes that generated the rhyolite of Glass Mountain, Medicine Lake volcano, N California. Contrib Mineral Petrol 127: 205–223.

Grove TL, Parman SW, Bowring SA, Price RC, Baker MB (2002) The role of an H2O-rich fluid component in the generation of primitive basaltic andesites and andesites from Mt. Shasta region, N California. Contrib Mineral Petrol 142: 375–396.

Hammarstrom JM, Zen EA (1986) Aluminum in hornblende: an empirical igneous geobarometer. Am Mineral 71: 1297-1313.

Hatherton T, Leopard AE (1964) The densities of New Zealand rocks NZ J Geol Geophys 7: 605-614.

Hayes G. Reyners M, Stuart G (2004) The Waiouru, New Zealand, earthquake swarm: persistent mid crustal activity near an active volcano. Geophys Res Lett 31: L19613.

Heiken G, Eichelberger JC (1980) Eruptions at Chaos Crags, Lassen Volcanic National Park, California. J. Volcanol. Geotherm Res 7:443–481.

Hill R, Roeder P (1974) The crystallization of spinel from basaltic liquid as a function of oxygen fugacity. J Geol 82: 709–729.

Hull AG, Dellow G (1993) Earthquake hazards in the Taranaki region. Institute of Geological and Nuclear Science Client Report 1993/03.

Hull AG (1994) Past earthquake timing and magnitude along the Inglewood Fault, Taranaki, New Zealand. Bull NZ National Earthquake Eng 16: 781-792.

Hunt TM, Woodward DJ (1971) Gravity and magnetic measurements in the South Taranaki Bight, New Zealand. NZ J Geol Geophys 14: 56-55.

Jackson MD, Cheadle MJ, Atherton MP (2003) Quantitative modeling of granitic melt generation and segregation in the continental crust. J Geophy Res 108: article 2332.

King PR, Thrasher GP (1996) Cretaceous-Cenozoic geology and petroleum systems of the Taranaki Basin, New Zealand. Institute of Geological and Nuclear Sciences Monograph 13: 243 pp

Lees CM, Neall VE (1993) Vegetation response to volcanic eruptions on Egmont Volcano, New Zealand, during the last 1500 years. J R Soc NZ 23: 91-127.

Legros F (2000) Minimum volume of a tephra fallout deposit estimated from a single isopach. J Volcanol Geotherm Res 96: 25-32.

Lipman PW, Mullineaux DR (1981) The 1980 eruptions of Mount St Helens. Washington. Geol Surv Prof Pap 1250 US Geol Survey, 844 pp.

Locke CA, Cassidy J (1997) Egmont Volcano, New Zealand: three-dimensional structure and its implications for evolution. J Volcanol Geotherm Res 76: 149-161.

Lowe DJ (1988) Stratigraphy, age, composition, and correlation of late Quaternary tephras interbedded with organic sediments in Waikato lakes, North Island, New Zealand. NZ J Geol Geophys 31: 125–165.

McKenzie D (1985) The extraction of magma from the crust and mantle. Earth Planet Sci Lett 74: 81–91.

McGlone MS, Neall VE, Clarkson BD (1988) The effects of recent volcanic events and climate changes on vegetation of Mt. Egmont (Mt. Taranaki), New Zealand. NZ J Bot 26: 123-144.

McGlone MS, Neall VE (1994) The late Pleistocene and Holocene vegetation history of Taranaki, North Island, New Zealand. NZ J Bot 32: 251-269.

Miyaji N (1988) History of Younger Fuji Volcano (in Japanese with English abstract). J Geol Soc Japan 94: 433–452.

Morgan DJ, Blake S, Rogers NW, De Vivo B, Rolandi G, Macdonald R, Hawkesworth CJ (2004) Timescales of crystal residence and magma chamber volume from modelling of diffusion profiles in phenocrysts: Vesuvius 1944. Earth Planet Sci Lett 222: 933–946.

Mortimer N, Tulloch AJ, Ireland TR (1997) Basement geology of Taranaki and Wanganui Basins, New Zealand. NZ J Geol Geophy 40: 223-236.

Mortazavi M, Sparks RSJ (2004) Origin of rhyolite and rhyodacite lavas and associated mafic inclusions of Cape Akrotiri, Santorini: the role of wet basalt in generating calcalkaline silicic magmas. Contrib Mineral Petrol 146: 397–413.

Neall VE (1972) Tephrochronology and tephrostratigraphy of western Taranaki (N108-109), New Zealand. NZ J Geol Geophys 18: 317-326.

Neall VE (1979) Sheets P19, P20 and P21 New Plymouth, Egmont and Manaia (1st Ed.) Geological Map of New Zealand 1:50 000, NZ DSIR, Wellington, scale 1:50 000, 3 sheets, pp. 36 text.

Neall VE, Stewart RB, Smith IEM (1986) History and Petrology of the Taranaki Volcanoes. R Soc NZ Bull 23: 251-263.

Norrish K, Hutton JT (1969) An accurate method for the analysis of a wide range of geological samples. Geochim Cosmochim Acta 33: 431-451.

Platz T (2007) Aspects of Dome-forming Eruptions from Andesitic Volcanoes through the Maero Eruptive Period (1000 yrs B.P. to Present) Activity at Mt. Taranaki, New Zealand. Unpub PhD thesis, Institute of Natural Resources, Massey University, Palmerston North, New Zealand.

Platz T, Cronin SJ, Smith IEM, Turner MB, Stewart RB (2007) Improving the reliability of microprobe-based analyses of andesitic glasses for tephra correlation. Holocene 17: 573-585 DOI: 10.1177/0959683607078982.

Price RC, Stewart RB, Woodhead JD, Smith IEM, (1999) Petrogenesis of high-K arc magmas: evidence from Egmont Volcano, North Island, New Zealand. J Petrol 40: 167-197.

Price RC, Gamble JA, Smith IEM, Stewart RB, Eggins S, Wnight IC (2005) An integrated model for the temporal evolution of andesites and rhyolites and crustal development in New Zealand's North Island. J Volcanol Geotherm Res 140: 1-24.

Prouteau G, Scaillet B (2003) Experimental constraints on the origin of the 1991 Pinatubo dacite. J Petrol 44: 2203–2241.

SAS Institute Inc (2004) SAS® Enterprise Guide® 3.0 Administrator: Users Guide. Cary NC: SAS Institute Inc. 160 pp.

Scandone R, Giacomelli L, Gasparini P (1993) Mount Vesuvius: 2000 years of volcanological observations. J Volcanol Geotherm Res 58: 5–25.

Shane P (2005) Towards a comprehensive distal andesitic framework for New Zealand based on eruptions from Egmont volcano. J Quat Sci 20: 45-57.

Sherburn S, White RS (2005) Crustal seismicity in Taranaki, New Zealand using accurate hypocentres from a dense network. Geophys J Int 162: 494-506.

Sherburn S, White RS (2006) Tectonics of the Taranaki region, New Zealand: earthquake focal mechanisms and stress axes. NZ J Geol Geophys 49: 269-279.

Sherburn S, White RS, Chadwick M (2006) Three-dimensional tomographic imaging of the Taranaki volcanoes, New Zealand. Geophy J Int 166: 957-969.

Sisson TW, Grove TL (1993) Experimental investigations of the role of H2O in calc-alkaline differentiation and subduction zone magmatism. Contrib Mineral Petrol 113: 143–166.

Smith DR, Leeman WP (1987) Petrogenesis of Mount St. Helens dacitic magmas. J Geophys Res 92: 10313–10334.

Sparks RSJ, Wilson L (1976) A model for the formation of ignimbrite by gravitational column collapse. J Geol Soc London 132: 441-451.

Stewart RB, Price RC, Smith IEM (1996) Evolution of high-K arc magma, Egmont volcano, Taranaki, New Zealand: Evidence from mineral chemistry. J Volcanol Geotherm Res 74: 275–296, doi: 10.1016/S0377-0273(96)00049-2.

Streck MJ, Dungan MA, Malavassi E, Reagan MK Bussy F (2002) The role of basalt replenishment in the generation of basaltic andesites of the ongoing activity at Arenal volcano, Costa Rica: evidence from clinopyroxene and spinel. Bull Volcanol 64: 316–327.

Tatsumi Y (1982) Origin of high-magnesian andesites in the Setouchi Volcanic Belt, Southwest Japan, 2. Melting phase-relations at high pressures. Earth Planet Sci Lett 60: 305–317

Tomiya A, Takahashi E (2005) Evolution of the magma chamber beneath Usu Volcano since 1663: A natural laboratory for observing changing phenocryst compositions and textures. J Petrol 46: 2395-2426.

Turner S, Evans P, Hawkesworth C (2001) Ultra-fast source-to-surface movement of melt at island arcs from 226Ra- 230Th systematics. Science 292: 136-1366

Turner MB, Bebbington MS, Cronin SJ, Stewart RB, (in press) Merging Eruption Datasets: Towards an Integrated Holocene Eruptive Record of Mt Taranaki, New Zealand, Bull Volcanol. accepted December 2008.

Turner MB, Cronin SJ, Smith IEM, Bebbington M, Stewart RB (2008a) Using titanomagnetite textures to elucidate volcanic eruption histories. Geology 36: 31-34.

Turner MB, Cronin SJ, Bebbington MS, Platz T (2008b) Developing a probabilistic eruption forecast for dormant volcanoes; a case study from Mt. Taranaki, New Zealand. Bull Volcanol 70: 507-515. DOI: 10.1007/s00445-007-0151-4.

Turner MB, Cronin, SJ, Smith IE, Stewart RB, Neall VE, (2008c) Eruption episodes and magma recharge events in andesitic systems; Mt Taranaki, New Zealand, J Volcanol Geotherm Res 177: 1063-1076.

Wilson CJN (1985) The Taupo eruption, New Zealand II. The Taupo ignimbrite. Phil Trans R Soc Lond A 314: 229-310.

Zernack A, Stewart RB, Price RC (2006) Slab or crust - K2O enrichment at Egmont volcano, New Zealand. Geochim Cosmochim Acta Suppl 70: 614.

Zellmer GF, Blake S, Vance D, Hawkesworth C, Turner S (1999) Plagioclase residence times at two island arc volcanoes (Kameni islands, Santorini, and Soufriere, St. Vincent) determined by Sr diffusion systematics. Contrib Mineral Petrol 136: 345-357.

Zellmer GF, Sparks RSJ, Hawkesworth CJ, Wiedenbeck M (2003) Magma emplacement and remobilization timescales beneath Montserrat: Insights from Sr and Ba zonation in plagioclase phenocryst. J Petrol 44: 1413-1431.